International Journal of Concrete Structures and Materials
DOI 10.1186/s40069-018-0247-6
ISSN 1976-0485 / eISSN 2234-1315

Two-Way Flexural Behavior of Donut-Type Voided Slabs

Joo-Hong Chung[1)], Hyung-Suk Jung[2),*], Baek-il Bae[1)], Chang-Sik Choi[3)], and Hyun-Ki Choi[4)]

(Received September 18, 2017, Accepted January 15, 2018)

Abstract: Voided slab systems were developed using segmented void formers such as spherical or oval plastic balls for two-way slab applications. This type of slab is expected to behave like a general two-way reinforced concrete slab because it has segmented voids, rather than the continuous voids of hollow core slabs. However, the structural behaviors of two-way voided slabs with segmented voids have not been clearly verified. Therefore, this paper analyzes the possibility of applying a donut-type two-way voided slab, which was investigated with a 12-point two-way bending test focused on global behaviors, including its load bearing capacity, flexural stiffness, ductility, deflection, and load distribution. In addition, the design method of a donut-type two-way voided slab was reviewed through the yield line method. The test results showed that one donut-type two-way voided slab acted like a conventional two-way reinforced concrete slab with the load distributed evenly between the different directions; however, another donut-type two-way voided slab with different characteristics showed uneven load distribution with different crack patterns. In addition, the yield line method could predict the load bearing capacities of the donut-type voided slabs with approximately 95% accuracy.

Keywords: voided slab, two-way flexural behavior, experimental investigation and load distribution.

1. Introduction

A voided slab is a reinforced concrete slab in which voids reduce the slab's weight. In this slab, lightweight void formers are placed between the top and the bottom reinforcements before concrete casting to replace concrete in the middle of the slab. In the early twentieth century, voided slab systems were developed using segmented void formers such as spherical or oval plastic balls for two-way slab applications. The segmented void formers are expected to eliminate the slab's directivity and reduce its weight while maintaining its flexural capacity. One of these slabs can reduce the slab weight by as much as 35% compared to a solid slab with the same flexural capacity (Mota 2010). For the advantages of voided slabs using segmented void formers, the concept and practice of voided slabs have been used, and various types of voided slabs have been developed currently.

Many tests have been conducted to evaluate the flexural capacities of voided slabs. In previous studies (BubbleDeck Technology 2008; Kim et al. 2009; Chung et al. 2010, 2014; Midkiff 2013), voided slabs showed similar strength and slightly lower stiffness compared to that of a solid slab with equal depth in analyses of one-way bending. Corey (2013) reported that the flexural strength of a voided slab with spherical voids is the same as that of a solid slab with equal depth if the compression block used to apply the bending force to the slab sections does not enter the void zone; and the flexural stiffness of this voided slab is approximately 80–90% of that of the solid slab due to the cross-sectional loss caused by voids.

These results were also demonstrated in analyses of two-way flexural capacities of voided slabs. As reported by Ibrahim et al. (2013), a voided slab with spherical voids behaved like a conventional two-way solid slab. The voided slab carried 89–100% of the ultimate load of a solid slab with equal depth, and showed slightly less stiffness than the solid slab. Wondwosen (2014) conducted finite element analysis of a voided slab with spherical voids, and reported that the in-plane bending stiffness of the voided slab decreased by 20% compared to that of a solid slab with equal depth. However, these researches focused on only the two-way flexural strength and stiffness of the voided slabs, without considering the load distribution through the different load-carrying directions.

The general assumption of a two-way slab design that the load will be distributed load-carrying directions has limited the acceptance of such two-way voided slabs since the two-way load distribution of the voided slabs has not been

[1)]Research Institute of Industrial Science, Hanyang University, Seoul 04763, Republic of Korea.
[2)]Department of Architectural Engineering, Catholic Kwandong University, Gangneung-si, Gangwon-do 25601, Republic of Korea.
*Corresponding Author; E-mail: junghs@cku.ac.kr
[3)]Division of Architectural Engineering, Hanyang University, Seoul 04763, Republic of Korea.
[4)]Department of Fire and Disaster Prevention Engineering, Kyungnam University, Changwon-si, Gyeongsangnam-do 51767, Republic of Korea.

Published online: 20 March 2018

verified yet. Therefore, this study investigates the directional load distribution in a two-way donut-type voided slab. In addition, this study introduces the effects of donut-type voids and the fixing device, which holds void formers in place, on the voided slab's structural behavior under two-way bending.

2. Experimental Program

2.1 Configuration of Two-Way Donut-Type Voided Slab Specimens

The objective of the flexural test was to evaluate the possibility of applying the donut-type voided slab as a two-way slab by comparing the resulting the load distribution, crack patterns, load-bearing capacity, flexural stiffness, and deflection with those of a solid slab with same tensile reinforcement ratio and dimensions.

To establish voids in the voided slab specimens, a donut-type void former was used, as shown in Fig. 1. The donut-type void former was a hexahedron with rounded edges and a hole penetrating the center. The void height and width were 140 and 270 mm, respectively. The hole diameter was 50 mm, and the distance between the voids was set to 30 mm in both the longitudinal and transverse directions.

To hold the donut-type void formers in place keeping them in the center of the slab's depth, two types of fixing methods were used: the spacer and the merged type, as shown in Fig. 2. The spacer-type consisted of void formers with protrusions, which acted as the spacers between the top and bottom rebars without requiring additional steel cages to hold the void formers. The merged-type held void formers using a steel cage, which was fabricated by welding the top and bottom rebars with D6 diagonal rebars.

The spacer-type fixing device does not affect the reinforcement ratio in either the longitudinal or transverse directions. In contrast, as shown in Fig. 3c, the legs of the merged-type fixing device increase the tensile reinforcement ratio in the B–B′ section, creating a relatively strong direction and a relatively weak direction in the voided slab specimen. Previous studies (Sagaseta et al. 2011; Matešan et al. 2012) have reported that different tensile reinforcement ratios in the longitudinal and transverse directions influence the flexural behavior of a slab under two-way bending. These reports motivated this investigation of the effect of the fixing methods on the structural behavior of the donut-type voided slabs.

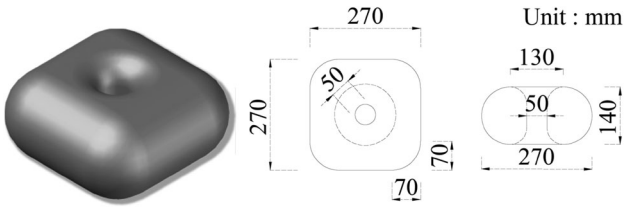

Fig. 1 Details of the donut type void former.

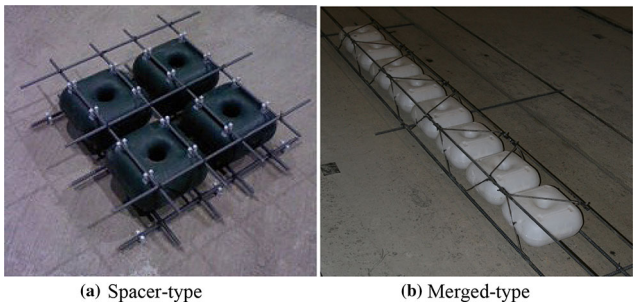

(a) Spacer-type (b) Merged-type

Fig. 2 Fixing methods of the donut type void formers.

Three test slabs were designed to investigate these effects: a conventional solid reinforced concrete slab (solid), a donut-type voided slabs with the spacer-type fixing method (TF–D–S–P.P), and a donut-type voided slabs with the merged-type fixing method (TF–D–M–P.P). The specimens were designed as square slabs with symmetric rebar arrangements. The widths and lengths of the slab specimens were 3300 mm, and their thicknesses were 250 mm. Twenty D10 and D13 rebar were symmetrically arranged in both the X- and Y-directions as the top and bottom rebars, respectively. In general, voided slabs are vulnerable to shear strength deterioration; hence, the slab specimens were designed to have low tensile reinforcement ratios (ρ) of 0.353% to induce flexural failure prior to shear failure. The merged-type fixing device was placed in the X-direction of the specimen. Detailed specifications of specimens are presented in Table 1 and Fig. 3.

2.2 Specimen Materials

Concrete used in all slab specimens came from one batch. The design strength of the concrete was 24 MPa, and the mixing ratio is summarized in Table 2. Five concrete cylindrical specimens were made with dimensions of 100 mm (diameter) × 200 mm (height), and then cured under the same conditions as that of the slab specimens. The concrete strength test conducted immediately before the structural test showed an average strength of 24.2 MPa, which was essentially equivalent to the design strength of 24 MPa.

For the rebar, D10 and D13 rebar with yield strength grades of 400 MPa were used as the top and bottom rebars, and D6 rebar with a yield strength grade of 440 MPa was used to fabricate the merged-type fixing devices. Tensile tests were conducted on the rebars, and the results are summarized in Table 3.

2.3 Loading and Measurement Set-Up

Previous studies (Sagaseta et al. 2011; Matešan et al. 2012; Fall et al. 2014) that conducted two-way bending tests used a pointed load at the center of the slab. However, with a pointed load, an unexpected punching shear failure could occur because of the concentration of shear stress around the loading point. Therefore, the application of multiple loading conditions was considered to provide better results, particularly in the case of voided slabs: voided slabs are vulnerable to the shear strength deterioration because they use of less concrete in the slab web and therefore less concrete is available to resist shear. For this reason, Ibrahim et al. (2013)

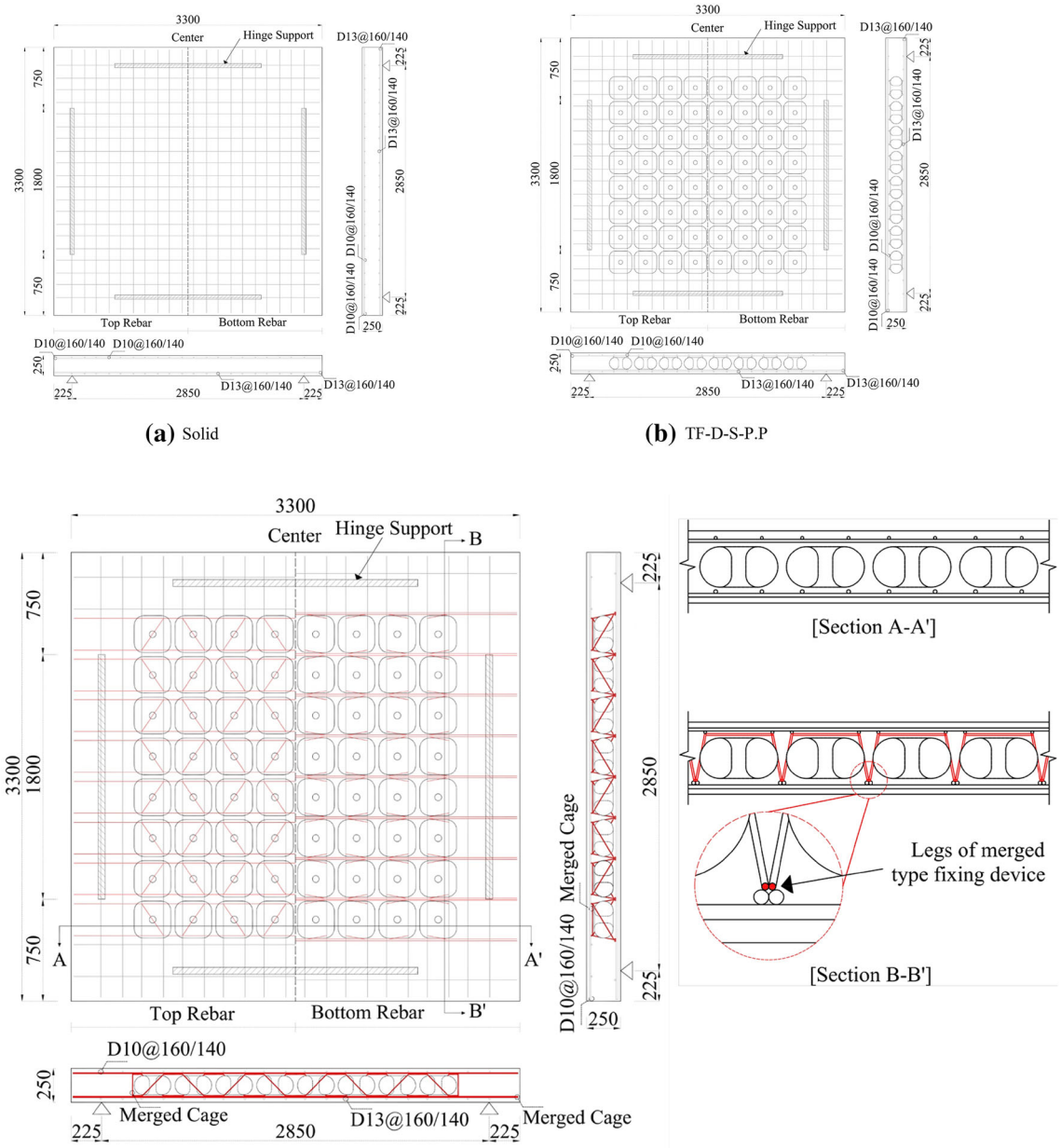

Fig. 3 Details of specimens.

tested a voided slab with spherical voids under a five-point loading system using five hydraulic jacks to avoid unexpected punching shear failure.

In this study, a 12-point loading system was used to apply the two-way bending test, as shown in Fig. 4, in order to avoid unexpected punching shear failure. The 12-point loading system consisted of one square and four triangular steel plates, twelve loading plates with dimensions of 200 mm × 200 mm, and sixteen steel ball bearings. To rotate freely with the slab deformation, the triangular steel plates were supported at only three points, each of them was connected with a ball bearing. The load generated by the actuator was first transferred directly to the center of the square steel plate, then transferred equally to the geometric centers of the four triangular steel plates, and then each of those loads was finally transferred equally to the three loading plates associated with each of the triangular plates.

The slab was supported at all edges with line-type reaction hinges with 1800 mm length to minimize experimental error from support conditions, such as the generation of fixed end moment, stress concentration, etc. The reaction hinges were located 225 mm apart from each end with a clear span of 2850 mm. Each reaction hinge was set up on a rubber sheet with a thickness of 10 mm above two steel frames that were arranged with 400 mm distances, and a load-cell was located between the two steel frames, as shown in Figs. 5 and 6.

Loading was implemented with a 2000 kN static-dynamic hydro-actuator with a loading speed of 1 mm/min. The load distributed toward each support was measured by a 1000 kN load cell installed beneath the center of the line-type reaction hinge. The deflection was measured by nine linear variable

Table 1 Details of specimens.

ID	Length × width × height (mm)	Clear span (mm)	Effect depth (mm)	Top rebar		Bottom rebar		Reinforcement ratio (%)		Void former		Fixing method type
				X-dir.	Y-dir.	X-dir.	Y-dir.	X-dir.	Y-dir.	Shape	Material	
Solid	3300 × 3300 × 250	2850 × 2850	217.3	20-D10		20-D13		0.353		–	–	–
TF–D–S–P.P										Donut	P.P	Spacer
TF–D–M–P.P								0.353 [0.40]	0.353			Merged

Where *TF* two-way flexure/*D* donut shaped void former/*P.P* polypropylene plastic, *S* spacer type fixing method, *M* merged type fixing method.
[ ] Considering the legs of the merged type fixing device.

differential transformers (LVDTs) placed under the intersection points of the slab's quartering lines in both directions, as shown in Fig. 6. The strain gauges were placed at the bottom rebars. For such simply-supported square slabs, the largest moments are generated along the diagonal axis, similar to the yield line. Therefore, the strain gauges on the bottom rebars were placed at the center and four corners of each slab specimen following the assumed yield line, as shown in Fig. 6.

2.4 Estimation of Load Bearing Capacity of Two-Way Slab Specimens

The ultimate load bearing capacities of slab specimens under two-way bending can be estimated based on the yield line theory. The yield line method uses rigid plastic theory to compute the failure loads corresponding to given plastic moment resistances in various parts of the slab (Johansen 1972; Hillerborg 1996; Wight and Macgregor 2012). The yield line method is a powerful method for predicting the failure load of reinforced concrete slabs (Bailey 2001; Famiyesin et al. 2001; Foster et al. 2004). Therefore, in this study, the ultimate load bearing capacities of specimens were estimated by the yield line method based on rigid plasticity theory as follows.

Failure mechanisms such as crack patterns and failure modes must be assumed to calculate the ultimate load-bearing capacities of specimens. In this study, considering the square shape of the slabs, the yield lines were assumed to form X-shapes along the diagonals between the unsupported corners, and the square slab was eventually divided into four-triangular parts, as shown in Fig. 7.

The external work (W_E) generated by the 12-point load is formulated by multiplying the external loads and displacements, as Eq. (1).

$$W_E = \left(\frac{P_u}{12}\right) \times (4 \times 0.8 + 8 \times 0.4) \times \delta_u \tag{1}$$

Here, P_u is the ultimate load; δ_u is the deflection at the center of slab under the ultimate load.

The internal work (W_I) generated by the in-plane moment along the yield line is formulated by multiplying the in-plane moment, the yield line length, and the rotation angle between two triangular plates along the yield line. The in-plane moment (m_b) per unit length along the yield line can be calculated by considering the moment equilibrium over per unit element of the slab, as shown in Eq. (2).

$$m_b = m_x \sin^2(\alpha) + m_y \cos^2(\alpha) \tag{2}$$

Here, α is the angle of the yield line; m_x and m_y are the in-plane moment per unit length resisted in the X- and Y-directions, respectively.

Both m_x and m_y can be calculated based on their respective section properties per unit length, following Eq. (3)

$$m_x = \rho_x d_x f_y (d_x - a_x/2) \text{ and } m_y = \rho_y d_y f_y (d_y - a_y/2) \tag{3}$$

The value of α can be assumed to be 45° because the specimens have square shapes and symmetric rebar arrangements; the

Table 2 Mix proportion of concrete and cylinder test results.

Cylinder test result	Design strength	W/C (%)	S/a (%)	Weight ratio (kg/m^3)				
				Water	Cement	Sand	Coarse aggregate	Admixture
24.2	24	56.6	47.4	193	341	837	985	1.7

Table 3 Mechanical properties of steel reinforcement.

Rebar type	Nominal strength (MPa)	Yield strength (MPa)	Yield strain (%)	Tensile strength (MPa)	Elongation (%)	Elastic modulus (GPa)
D10	400	469	0.20	648	17.36	196.1
D13	400	473	0.24	665	18.21	194.3
D6	440	528	0.26	675	15.28	205.8

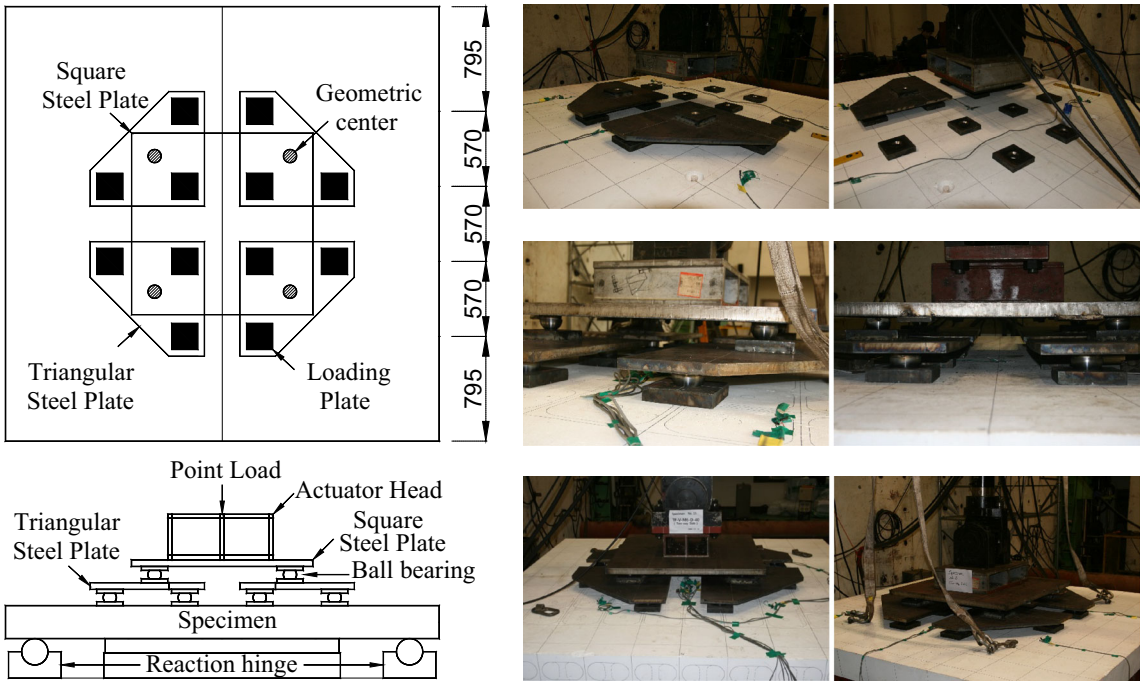

Fig. 4 Installation of 12-point loading system (unit: mm).

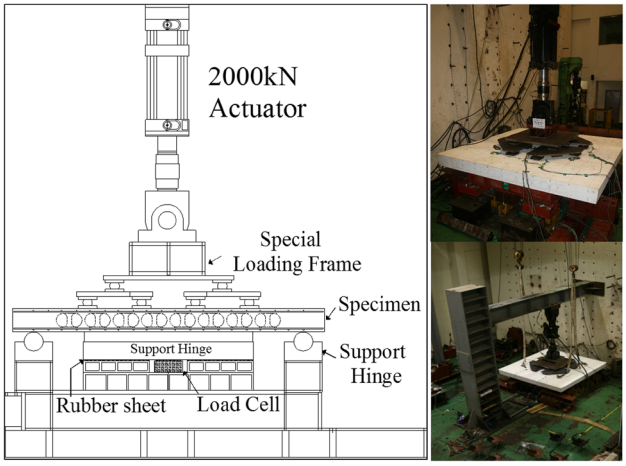

Fig. 5 Test set-up (overall).

tensile reinforcement ratio (ρ), effective depth (d), and the depth of the equivalent rectangular stress block (a) can be assumed to be the same in both X- and Y-directions because their difference in these directions are small. Based on the full slab length (L_f), the total yield line length can be defined as $2\sqrt{2}\,L_f$. The rotation angle (θ_u) between two triangular plates along the yield line can be calculated using Eq. (4), assuming the angle is small (see Fig. 7).

$$\theta_u = \frac{2\sqrt{2}\delta_u}{L_n} \tag{4}$$

Here, L_n is the net length between simple supports, as shown in Fig. 7.

Through Eqs. (2)–(4), the internal work (W_I) can be calculated by Eq. (5).

$$W_I = 2\sqrt{2}L_f \times m_b \times \theta_u = 8m_b\frac{L_f}{L_n}\delta_u \tag{5}$$

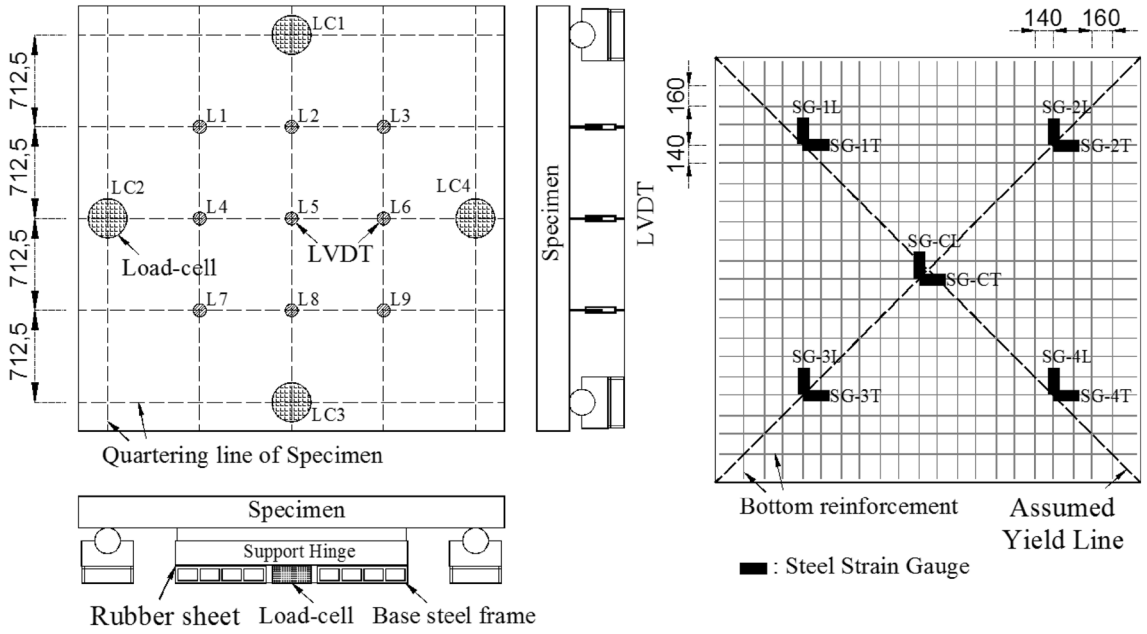

Fig. 6 Details of measurement plan (unit: mm).

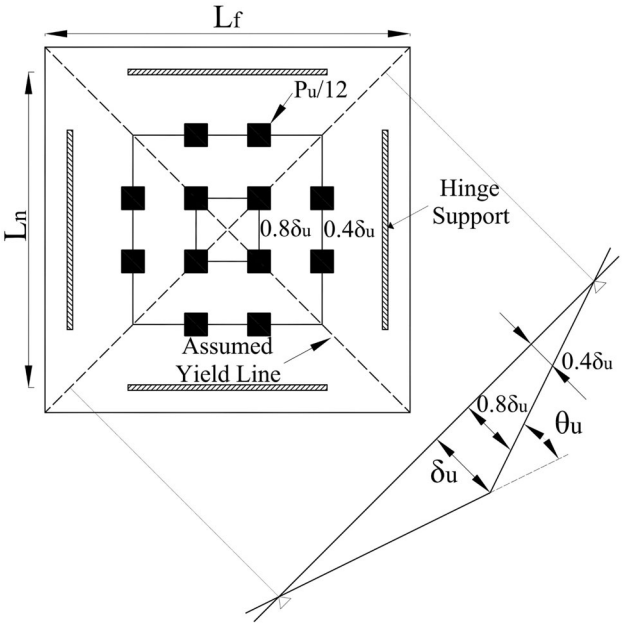

Fig. 7 Assumed yield line and failure mode.

According to the energy conservation principle, the external work and internal work should be equal; therefore, the specimen's ultimate load bearing capacity (P_u) is calculated to be 1119 kN using Eq. (6).

$$P_u = 15 m_b \frac{L_f}{L_n} \tag{6}$$

3. Test Results and Discussion

3.1 Global Failure Behavior

All of the slabs showed typical flexural behavior under two-way bending: maintaining an elastic state until cracking, inelastic behavior after cracking, and failure with concrete crushing at the top of the slab surface after the bottom rebars yielded.

As shown in Fig. 8, the solid slab showed ductile flexural behavior with yielding of bottom the rebars, and the donut-type voided slabs also showed ductile flexural behavior regardless of the fixing method. The displacement-ductility ratio of the donut-type voided slabs ($\mu = 3.4$ and 4.1) were also comparable to that of the solid slab ($\mu = 4.4$).

3.2 Load Bearing Capacity

As expected, the load bearing capacities of donut-type voided slabs were similar to that of the solid slab. As shown in Table 4, the yield load and initial cracking load of TF–D–S–P.P were similar to those of the solid slab. TF–D–M–P.P was similar in the yield load but higher in the initial cracking load compared to the solid slab. The yield load was defined as the load at which one of the bottom rebars reached the yield strain of 0.24%. The initial cracking load was defined as the load at which the strain on one of the bottom rebars increased suddenly in the elastic state.

The ultimate load-bearing capacities of TF–D–S–P.P and TF–D–M–P.P were equivalent to 95 and 99% of that of the solid slab, respectively. Table 4 shows that the ultimate load bearing capacity of TF–D–M–P.P was approximately 5% higher than that of TF–D–S–P.P. Although this is only a slight difference, it is inferred to be enabled by the legs of the merged-type fixing device resulted in an increased tensile reinforcement ratio. The legs of the merged-type fixing device increase the tensile reinforcement ratio by 0.40% in the longitudinal direction of the merged-type fixing device (X-direction of specimen).

If the effect of the merged-type fixing device on the increased tensile reinforcement ratio is considered, the load bearing capacity of TF–D–M–P.P calculated by the yield line method is 1172 kN, an approximately 5% increase over

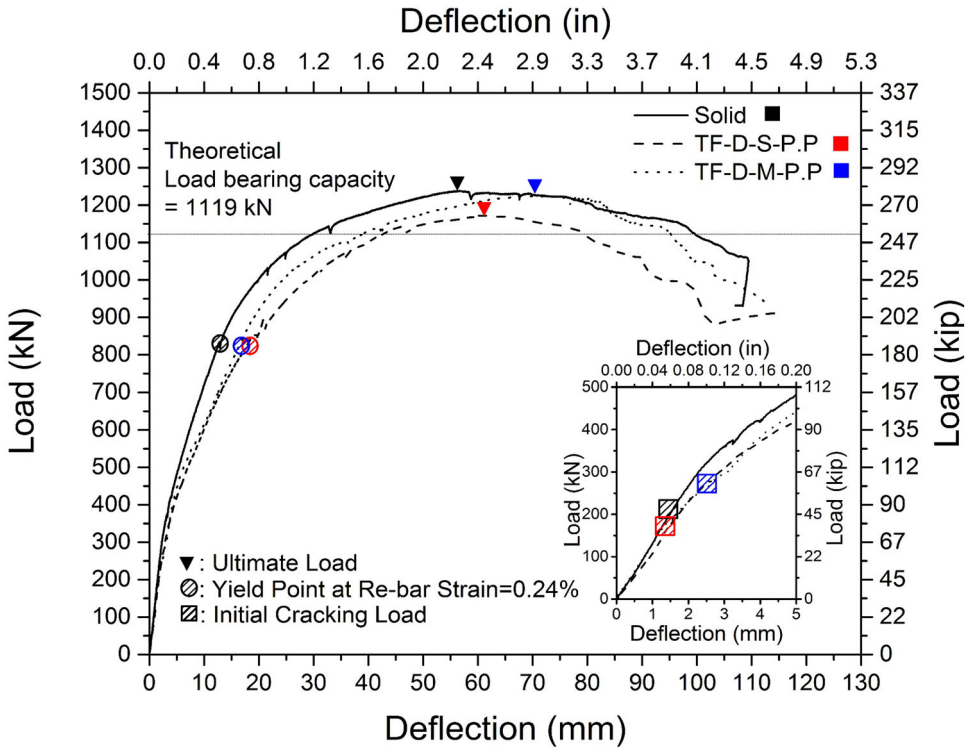

Fig. 8 Load–deflection curve.

1119 kN, which is the load bearing capacity of TF–D–S–P.P calculated by the same method. In other words, the calculations show the same tendency as the experimental result. Therefore, the increased tensile reinforcement ratio due to the merged-type fixing device needs to be considered with regard to the load bearing capacity of this type of voided slab.

When the load bearing capacity of the donut-type voided slab was evaluated by the yield line method, the load bearing capacity could be predicted with approximately 95% accuracy. Therefore, the yield line method can be applied to calculate the load bearing capacity of the donut-type voided slab under two-way bending, as in similar analyses of the conventional solid slab.

3.3 Flexural Stiffness

As shown in Fig. 8, the flexural stiffness of the donut-type voided slabs decreased compared to that of the solid slab, although the flexural stiffness of the donut-type voided slab was improved slightly with the merged-type fixing method. For each specimen, the flexural stiffness and the effective moment of inertia (I_e) were compared to evaluate the flexural stiffness of the donut-type voided slab. The flexural stiffness was compared through the secant stiffness (K) under a yield load and was calculated by Eq. (7).

$$K = \frac{P_y}{\delta_y} \tag{7}$$

As shown in Table 4, the secant stiffness of the donut-type voided slabs were lower than that of the solid slab, with stiffness decreases of 27 and 23% for TF–D–S–P.P and TF–D–M–P.P, respectively. The decreased secant stiffness of the donut-type voided slabs is attributable to the cross-sectional loss caused by voids inside the slab. However, the secant stiffness of TF–D–M–P.P and TF–D–S–P.P also differed, even though these slabs had the same cross section. The secant stiffness of TF–D–M–P.P was 7% higher than that of TF–D–S–P.P, which may have been caused by the increased the tensile reinforcement ratio due to the merged-type fixing device.

To confirm this conjecture, the effective moment of inertia of the specimens were compared under a yield load. The effective moment of inertia was initially proposed by Branson (1977), with the intention of reflecting the loss of concrete cross section according to crack propagation. As shown in Eq. (8), the effective moment of inertia is calculated using the uncracked moment of inertia (I_g), the cracked moment of inertia (I_{cr}), and the flexural cracking moment (M_{cr}).

$$I_e = I_{cr} + \left(\frac{M_{cr}}{M_a}\right)^3 (I_g - I_{cr}) \quad \leq I_g \tag{8}$$

As shown in Fig. 9, the effective moment of inertia of the voided slab was calculated for the cross section passing through the center of the donut-type voids. In the case of TF–D–M–P.P, the increased tensile reinforcement ratio due to the merged-type fixing device was considered to calculate the effective moment of inertia.

The uncracked moment of inertia of the donut-type voided slab ($I_{g,D}$) was calculated using Eqs. (9) and (10), in consideration of the cross-sectional loss of concrete due to the voids. The cracked moment of inertia of the donut-type voided slab ($I_{cr,D}$) was assumed to be 90% of the cracked moment of inertia of the solid slab ($I_{cr,S}$) based on the results

Table 4 Test results of specimens.

ID	Calculation		Test results						Comparison			
	P_n kN	I_e $\times 10^6$ mm^4	P_{cr} kN	δ_{cr} mm	P_y kN	δ_y mm	P_u kN	δ_u mm	μ	K kN/mm	$\frac{P_u}{P_n}$	$\frac{P_u}{P_{u,Solid}}$	$\frac{K}{K_{Solid}}$	$\frac{I_e}{I_{e,Solid}}$
Solid	1119	2101	205.9	1.53	824.1	12.95	1238.5	56.60	4.4	5.27	1.10	–	–	–
TF–D–S–P.P		1643	170.8	1.45	823.3	17.77	1172.5	60.69	3.4	6.85	1.05	0.95	0.73	0.78
TF–D–M–P.P	1172	1798	284.7	2.78	847.8	17.16	1225.1	70.50	4.1	6.54	1.05	0.99	0.78	0.86

P_n Ultimate flexural load calculated with the yield line method
P_{cr} Load at initial flexural crack occurred deduced by strain of bottom rebar
P_y Load when one of bottom rebar strain is reached by 0.24%
δ_{cr} Deflection at the center under cracking load / δ_y Deflection at the yield load

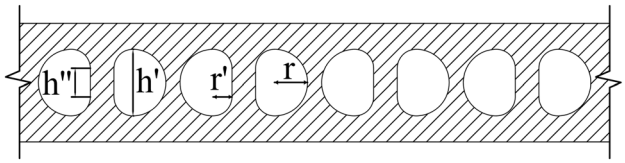

Fig. 9 Assumed section of the donut-type voided slab for calculating the moment of inertia.

of previous researches (BubbleDeck Technology 2008; Midkiff 2013), as shown in Eq. (11).

$$I_{g,D} = I_{g,S} - N(I_D) \tag{9}$$

$$I_D = \frac{\pi r^4}{4} + \frac{r' h''^3}{6} + \left(\frac{\pi r'^4}{4} + \pi r'^2 \left(\frac{h''}{2} + \frac{4r'}{3\pi}\right)^2\right) \tag{10}$$

$$I_{cr,D} = 0.9 I_{cr,S} \tag{11}$$

In these equation, $I_{g,S}$ is the uncracked moment of inertia of the solid slab's cross section considering rebar; I_D is the moment of inertia of a void; $I_{cr,S}$ is the cracked moment of inertia of the solid slab's cross section; N is the number of voids in the calculated section; and the others values are shown in Fig. 9.

Table 4 presents the effective moment of inertia about Y-axis of each slab under a yield load. Comparing the specimens, the effective moments of inertia of TF–D–S–P.P and TF–D–M–P.P were lower than that of the solid slab by 22 and 14%, respectively. In addition, the effective moment of inertia of TF–D–M–P.P was approximately 10% higher than that of TF–D–S–P.P. These results of the effective moment of inertia show the similar tendency as the experimental result of the secant stiffness. Therefore, the cross-sectional loss caused by voids and the increased tensile reinforcement ratio due to the merged-type fixing device need to be considered with regard to the flexural stiffness of this type of voided slab.

3.4 Crack Pattern

Figure 10 shows the crack patterns on the bottom surfaces of the slabs. In general, diagonal cracks formed in an X-shape ranging from the center of the slab toward the unsupported corners, following the assumed yield lines.

In the solid slab, several diagonal cracks with large widths were observed between the unsupported corners and multiple diagonal cracks with small widths were diffused beside the large diagonal cracks. Very few orthogonal cracks with large widths were observed; only some orthogonal cracks with small widths were formed in the center of the slab and near the supports. The number of cracks in the solid slab was relatively higher than those in the donut-type voided slabs; however, most of these cracks had small widths, as shown in Fig. 10a.

In TF–D–S–P.P, the crack pattern was similar to that of the solid slab: several large-width diagonal cracks between the unsupported corners. However, only a few small-width diagonal cracks were observed in TF–D–S–P.P, and the spacing of the large-width diagonal cracks was relatively

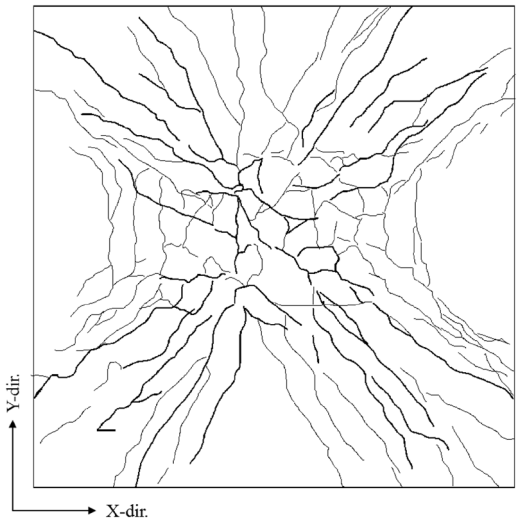

(a) Solid

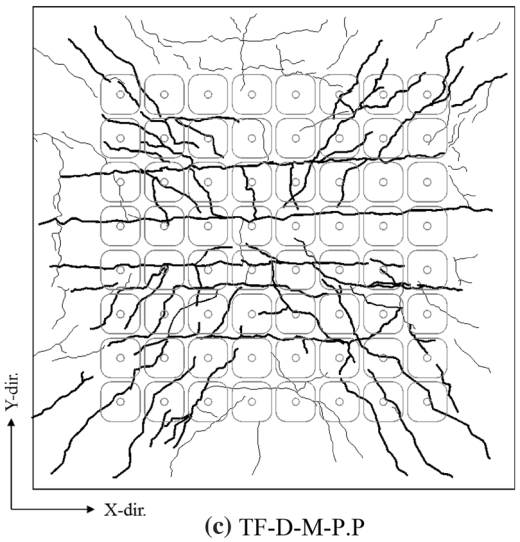

(c) TF-D-M-P.P

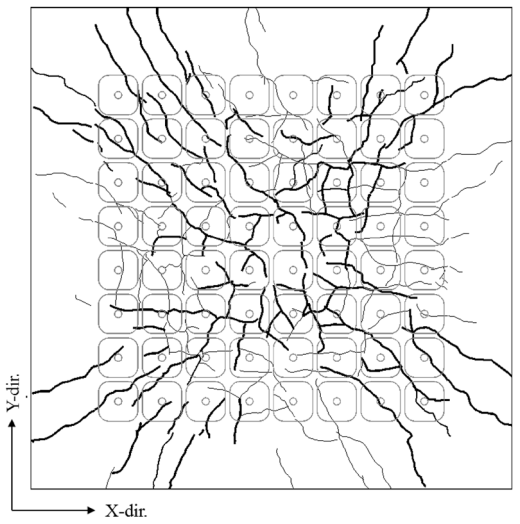

(b) TF-D-S-P.P

Fig. 10 Crack patterns on bottom surface of slabs.

large in comparison to that of the solid slab, as shown in Fig. 10b.

In TF–D–M–P.P, the diagonal crack pattern was similar to that of TF–D–S–P.P. TF–D–M–P.P also showed large-width diagonal cracks and a few small-width diagonal cracks between the unsupported corners, with relatively large crack spacing. However, large-width orthogonal cracks were observed parallel to the merged-type fixing device direction, as shown in Fig. 10c. These cracks were inferred to be enabled by the merged-type fixing device. In general, in a square slab with a symmetrical rebar arrangement, orthogonal cracks do not propagate. Only diagonal cracks propagate along the yield line, as occurred in the solid and TF–D–S–P.P slabs. In contrast, in a slab with an asymmetrical rebar arrangement, the cracks propagate perpendicular to the weak direction (Sagaseta et al. 2011; Matešan et al. 2012; Fall et al. 2014). The legs of the merged-type fixing device increase the tensile reinforcement ratio by 0.40%, creating a strong direction and a weak direction, relative to one another. As a result, the orthogonal cracks propagated parallel to the direction of the merged-type fixing device in TF–D–M–P.P.

3.5 Strain of Bottom Reinforcement Bars

In reinforced concrete flexural members, the rebar behavior can show the failure mechanism clearly. Therefore, the strains of the bottom rebars in both the X- and Y-directions at five points, located at the center and four corners of each slab specimen (along with the assumed yield lines), were examined. The load-rebar strain relationships of all specimens are presented in Fig. 11.

In the solid slab, there was little difference in the rebar behavior for rebars arranged in different directions; however, the rebar behavior could be divided into two groups according to location. Rebars located at the center of the slab deform earlier with cracking and start to yield at a significantly lower load, compared to rebars at the corners of the slab. Therefore, the deformation of the slab can be deduced to begin at the center, and then spread toward the corners, and the solid slab behaved symmetrically in both the X- and Y-directions under two-way bending.

In TF–D–S–P.P, the rebar behavior was very similar to that of the solid slab: the behavior of rebars could also be divided into two groups by location, and the rebar behaviors in both X- and Y-directions were almost the same. There was just one noticeable difference between the solid slab and TF–D–S–P.P: in TF–D–S–P.P, the rebars located at the corners began to yield at a slightly lower load than in the solid slab. However, this difference was minor in comparison with the ultimate load. Therefore, the donut-type voided slab with the spacer-type fixing method can be considered to behave symmetrically in both the X- and Y-directions, like a conventional solid slab under two-way bending.

In contrast, in TF–D–M–P.P, the rebar behavior was quite different from that in the solid slab and TF–D–S–P.P. In TF–D–M–P.P, the rebar behavior cannot be easily divided into two-groups by location, even though the rebars at the center of the slab yielded first. However, the rebar behavior in both the X- and Y-directions were clearly different. The rebars in the Y-direction had a tendency to yield at a relatively lower load compared to that of the rebars in the X-direction. This result is expected to be caused by the legs of the merged-type fixing device, which create relatively weak and strong

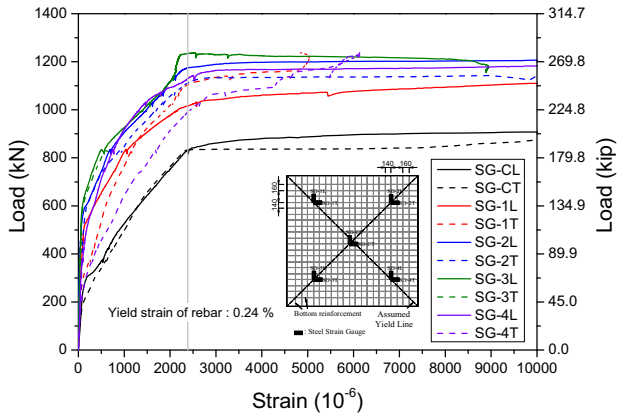

(a) Solid

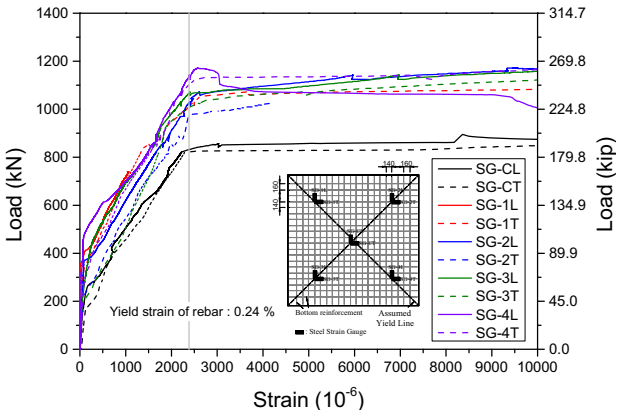

(b) TF-D-S-P.P

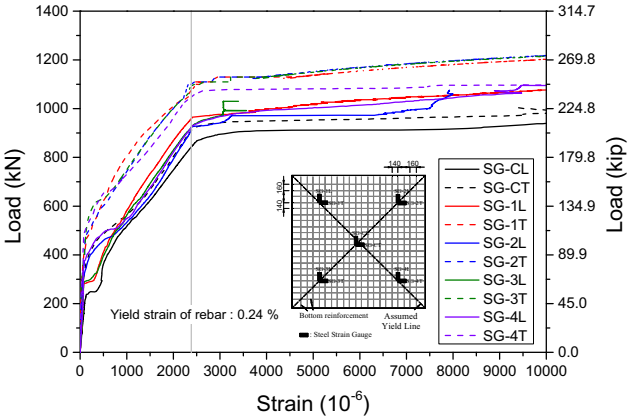

(c) TF-D-M- P.P

Fig. 11 Load–rebar strain of two-way slab specimens.

directions, as discussed above. Hence, the deformation was concentrated along the weak direction of the Y-axis in this specimen.

Based on these results, the failure behavior of TF–D–M–P.P can be verified. At the initial loading stage before the rebar yielded, the slab behaved symmetrically with diagonal cracks like the solid slab, and then the rebars in the Y-direction began to yield earlier than that in X-direction. Thus, the load was redistributed to the unyielding rebars in X-direction, and as a result, the load increased even more after the rebars yielded in Y-direction.

3.6 Deflection Distributions in Both X- and Y-Directions

In order to investigate the slab deflections along both the X- and Y-directions, measurements from the lines formed by the LVDTs 4, 5, 6 and LVDTs 2, 5, 8 were compared at four loading stages: $0.25P_u$, $0.50P_u$, $0.75P_u$, and $1.0P_u$. The deflection distributions in both the X- and Y-directions as the load increased are presented in Fig. 12.

The solid slab and TF–D–S–P.P showed almost equivalent deflection distributions along both the X- and Y-directions until the ultimate load. In contrast, TF–D–M–P.P showed different deflection distributions in both the X- and Y-directions. The deflection distributions of these two directions were almost the same until the load reached $0.5P_u$. However, the deflection in the Y-direction was larger than that in the X-direction after the yielding of the rebars arranged in the Y-direction, and then at $1.0P_u$, the deflection in the Y-direction became significantly larger than that in the X-direction, as shown in Fig. 12c. The difference in the deflection distributions between the two directions was caused by the early yielding of the Y-direction rebar. After the yielding of the Y-direction rebar, the deflection would be increased significantly along in the Y-direction with even a small load increase.

3.7 Load Distributions in Both X- and Y-Directions

A two-way slab is established under the assumption that the load will be distributed through both the X- and Y-directions, and the load distribution ratio between the different load-carrying directions is used in current design methods. The load distribution ratio in two directions is simply calculated under a few basic assumptions:

(1) Each load, which is distributed between different load-carrying directions, works only in one direction, although the slab behavior under two-way bending results from complex interactions between the flexural behaviors in each direction; and (2) the deflection at the center of the slab should always be identical regardless of the directions.

The deflection of a two-way slab is related to the amount of load, the material's elastic modulus (E), and geometrical properties such as the length (L) and moment of inertia of a section in the load-carrying direction (I). In general, the deflection at the center of a slab (δ_c) along each direction under a distributed load (ω) is calculated with Eq. (12).

$$\delta_c = \frac{5\omega L^4}{384EI} \tag{12}$$

Assuming that the material properties are identical in both directions, the load distribution ratio between the different load-carrying directions can be obtained by Eq. (13) because the deflection at the center of a slab in both directions should be equal.

$$\frac{\omega_x}{\omega_y} = \frac{I_x}{I_y}\frac{L_y}{L_x} \tag{13}$$

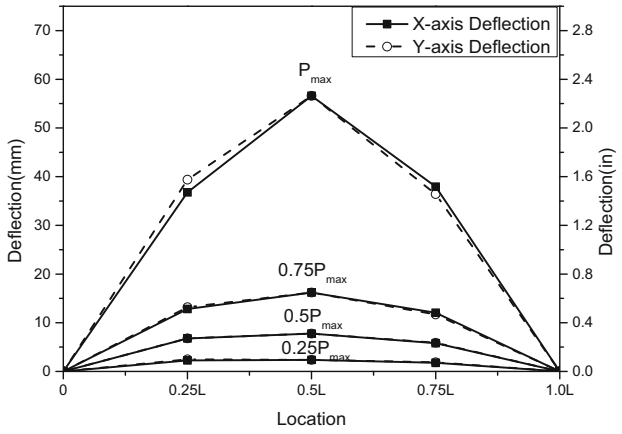

(a) Solid

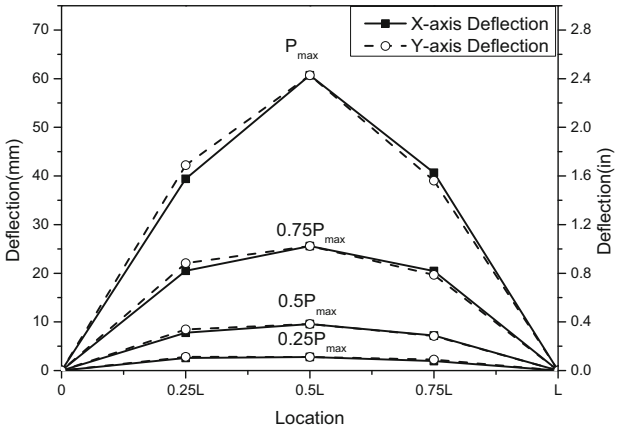

(b) TF-D-S-P.P

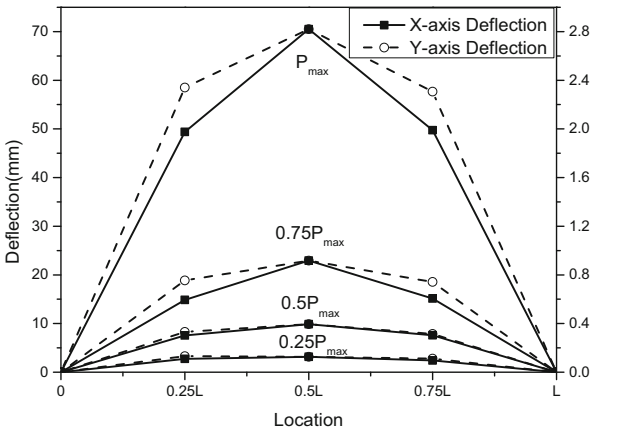

(c) TF-D-M- P.P

Fig. 12 Deflection distributions of two-way slab specimens.

To summarize, the proportion of the distributed load in each direction is directly proportional to the ratio of their moment of inertia and inversely proportional to the ratio of their length. The case of a square slab is more simplified because the length ratio is unity. Therefore, the load is theoretically distributed equally in both directions in the case of a square slab with a symmetrical rebar arrangement, like the solid slab and TF–D–S–P.P.

To evaluate the load distribution in the donut-type voided slab, measurements from four load-cells placed under the centers of the support hinges were compared at four loading stages: $0.25P_u$, $0.50P_u$, $0.75P_u$, and $1.0P_u$. It is impossible to measure the total distributed load at each support because the hinges supported not only load-cells, but also steel beams to secure stability. Therefore, the ratio of each load-cell's measured value to the sum of the measured values for all load-cells were compared to evaluate the load distribution of

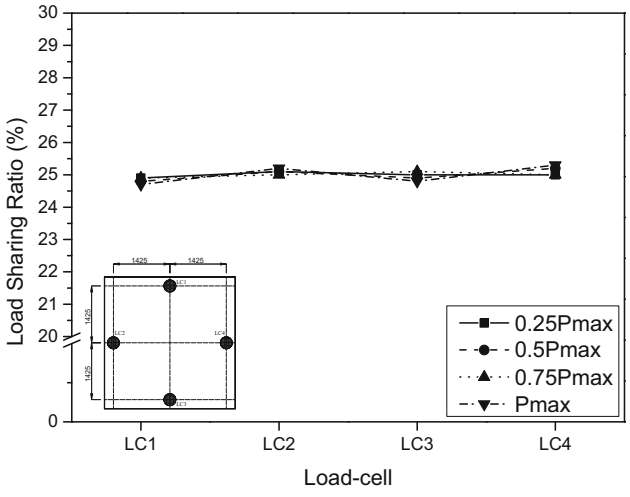

(a) Solid

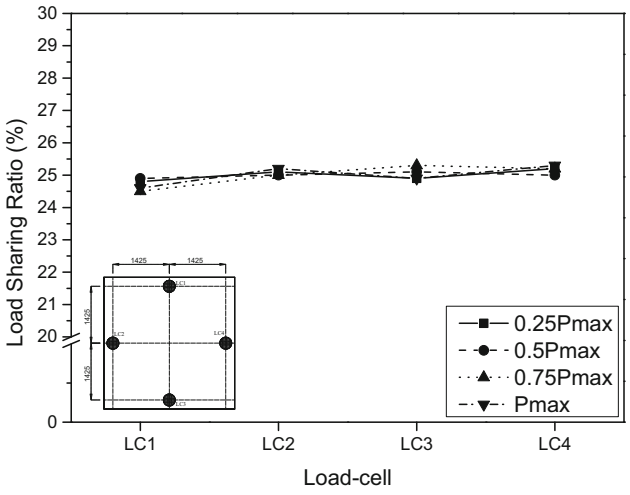

(b) TF-D-S-P.P

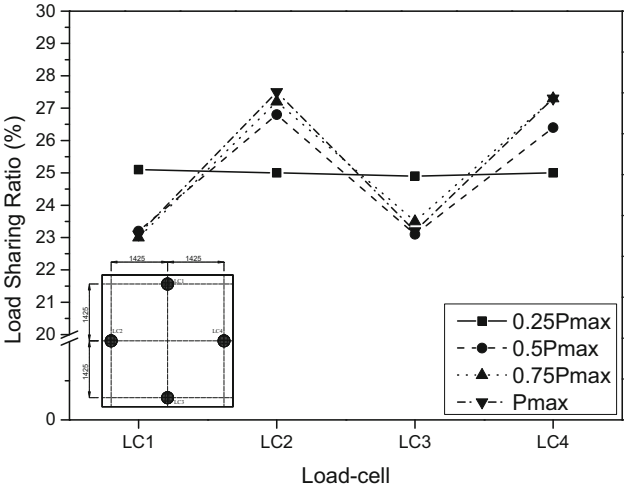

(c) TF-D-M- P.P

Fig. 13 Load sharing ratios of two-way slab specimens.

the slab under two-way bending. The results are summarized in Fig. 13.

The load-sharing ratios in both the X- and Y-directions were almost equivalent to each other until the ultimate load in the specimens with the symmetric rebar arrangement (the solid slab and TF–D–S–P.P). In contrast, TF–D–M–P.P showed different load-sharing ratios in the two directions with increasing load. The load-sharing ratios in these two directions were almost the same until the load reached $0.25P_u$ before cracking. However, the load-sharing ratio in the X-direction was larger than that in the Y-direction after the cracking, and then the load-sharing ratio in the X-direction gradually increased until the load reached ultimate load, as shown in Fig. 13c. The different load-sharing ratios in the two directions are expected to be caused by the different moment of inertia in the two directions. The donut-type voided slab with the merged-type fixing device has a larger effective moment of inertia in the X-direction compared to that in the Y-direction. Therefore, the different effective moment of inertia in both two directions is expected to have caused the different load-sharing ratios in two directions.

4. Conclusion

To evaluate the possibility of applying the donut-type voided slab as a two-way slab, the structural behavior of the donut type voided slab, including its load bearing capacity, flexural stiffness, ductility, deflection, and load distribution, were investigated. The following conclusions can be drawn from the results of the experimental tests of the donut-type voided slab under two-way bending.

(1) The donut-type voided slab showed typical two-way flexural behavior, with diagonal cracks formed in an X-shape ranging from the center of the slab toward the unsupported corners. Compared to a conventional solid slab, the spacing of the diagonal cracks was relatively large, and only a few small-width diagonal cracks were observed in donut-type voided slab. In addition, the donut-type voided slab with the merged-type fixing device showed large-width orthogonal cracks, parallel to the merged-type fixing device direction.

(2) In terms of load bearing capacity, the donut-type voided slabs demonstrated comparable load bearing capacities to that of the solid slab with the same reinforcement ratio. The application of the merged-type fixing device increased the load bearing capacity of the donut-type voided slab by approximately 5%, which was attributed to the improved tensile reinforcement ratio introduced by the legs of the merged-type fixing device.

(3) In terms of flexural stiffness, the donut-type voided slabs demonstrated lower flexural stiffness than that of the solid slab with the same reinforcement ratio. The decrease in the flexural stiffness of the donut-type voided slab was caused by the reduced effective moment of inertia introduced by the voids. In addition, the merged-type fixing device affected the effective moment of inertia of the donut-type voided slab by changing the reinforcement ratio. Therefore, the geometrical properties of the voids and the fixing device should be considered when analyzing the flexural stiffness of the donut-type voided slabs under two-way bending.

(4) In terms of ductility, the donut-type voided slabs showed displacement ductility ratios of 3.4–4.1. These values were comparable to that of the solid slab. Therefore, the two-way donut-type voided slabs were considered to have sufficient ductility to perform as general flexural members.

(5) In terms of the deflection distribution, the donut-type voided slabs demonstrated equivalent deflection distribution in both the X- and Y-directions. However, the donut-type voided slab with the merged-type fixing device demonstrated an asymmetric deflection distribution, which could be regarded as a typical behavior for two-way slab with asymmetric rebar arrangements.

(6) In terms of load distribution, the donut-type voided slabs demonstrated equivalent load distributions in both the X- and Y-direction. The donut-type voided slab with the merged-type fixing device demonstrated different load distributions in the X- and Y-directions, which as with the deflection result, could be regarded as a typical behavior for two-way slabs with asymmetric rebar arrangements.

(7) In this study, the yield line method was reviewed for designing a donut-type two-way voided slab. As a result, the yield line method demonstrated a prediction accuracy of as high as 95% in the ultimate load bearing capacity. Therefore, the yield line method can be applied to design of the donut-type voided slab under two-way bending, as in similar analyses of the conventional solid slab.

(8) Based on the test results and evaluations, the donut-type voided slab can be applied as a two-way slab in place of the conventional heavy solid slab.

Acknowledgements

This work was supported by the National Research Foundation of Korea (NRF) Grant funded by the Korea Government (MSIP) (No. NRF-2016R1C1B1012618).

References

Bailey, C. G. (2001). Membrane action of unrestrained lightly reinforced concrete slabs at large displacements. *Engineering Structures, 23,* 470–483.

Branson, D. E. (1977). *Deformation of concrete structures* (p. 1977). New York: McGraw-Hill Book Co.

BubbleDeck Technology. (2008). *BubbleDeck voided flat slab solutions—Technical manual & documents*. Delta: BubbleDeck UK.

Chung, J. H., Choi, H. K., Lee, S. C., & Choi, C. S. (2014). Flexural strength and stiffness of biaxial hollow slab with donut type hollow sphere. *AIK Journal, Korea, 30*(5), 3–11.

Chung, L., Lee, S.-H., Cho, S.-H., & Woo, S.-S. (2010). Investigations on flexural strength and stiffness of hollow slabs. *Advances in Structural Engineering, 13*(4), 591–601.

Corey, J. M. (2013). *Plastic voided slab systems: Applications and design*. Manhattan, KS: Kansas State University.

Fall, D., Shu, J., Rempling, R., Lundgren, K., & Zandi, K. (2014). Two-way slabs: Experimental investigation of load redistributions in steel fibre reinforced concrete. *Engineering Structures, 80,* 61–74.

Famiyesin, O. O. R., Hossain, K. M. A., Chia, Y. H., & Slade, P. A. (2001). Numerical and analytical predictions of the limit load of rectangular two way slabs. *Computers & Structures, 79,* 43–52.

Foster, S., Bailey, C., Burgess, I., & Plank, R. (2004). Experimental behaviour of concrete floor slabs at large displacements. *Engineering Structures, 26*(2), 1231–1247.

Hillerborg, A. (1996). *Strip method design handbook*. London: E & FN Spon.

Ibrahim, A. M., Ali, N. K., & Salman, W. D. (2013). Flexural capacities of reinforced concrete two-way bubbledeck slabs of plastic spherical voids. *Diyala Journal of Engineering Sciences, 6*(2), 9–20.

Johansen, K. W. (1972). *Yield-line formulae for slabs*. London: Cement and Concrete Association. ISBN 0-7210-0819-4.

Kim, S. M., Jang, T. Y., & Kim, S. S. (2009). Structural performance tests of two-way void slabs. *AIK Journal, Korea, 25*(8), 35–42.

Matešan, D., Radnić, J., Grgić, N., & Čamber, V. (2012). Strength capacity of square reinforced concrete slabs. *Materials Science & Engineering Technology, 43*(5), 399–404.

Mota, M. (2010). Voided slabs: Then and now. *Concrete International, 32*(10), 41–45.

Sagaseta, J., Muttoni, A., Fernandez Ruiz, M., & Tassinari, L. (2011). Non-axis-symmetrical punching shear around internal columns of RC slabs without transverse reinforcement. *Magazine of Concrete Research, 63*(6), 441–457.

Wight, J. K., & Macgregor, J. G. (2012). *Reinforced concrete: Mechanics and design* (6th ed.). London: Pearson Education Inc. ISBN 978-0-13-217652-1.

Wondwosen, B. A. (2014). *Two dimensional micromechanics based on computational model for spherically voided biaxial slabs (SVBS)*. Fairfax, VA: George Mason University.